

# Surface Adatom Diffusion-Assisted Dislocation Nucleation in Metal Nanowires

Lijie He, Guangming Cheng, Yong Zhu, and Harold S. Park\*



Cite This: *Nano Lett.* 2023, 23, 5779–5784



Read Online

ACCESS |



Metrics & More



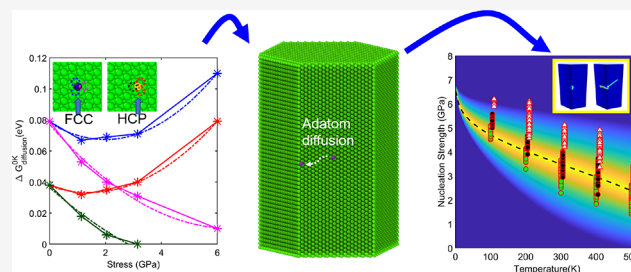
Article Recommendations



Supporting Information

**ABSTRACT:** We employ a hybrid diffusion- and nucleation-based kinetic Monte Carlo model to elucidate the significant impact of adatom diffusion on incipient surface dislocation nucleation in metal nanowires. We reveal a stress-regulated diffusion mechanism that promotes preferential accumulation of diffusing adatoms near nucleation sites, which explains the experimental observations of strong temperature but weak strain-rate dependence as well as temperature-dependent scatter of the nucleation strength. Furthermore, the model demonstrates that a decreasing rate of adatom diffusion with an increasing strain rate will lead to stress-controlled nucleation being the dominant nucleation mechanism at higher strain rates. Overall, our model offers new mechanistic insights into how surface adatom diffusion directly impacts the incipient defect nucleation process and resulting mechanical properties of metal nanowires.

**KEYWORDS:** mechanical deformation, plasticity, surface diffusion, defect nucleation, nanostructures, kinetic Monte Carlo



With the continuous development of experimental technologies such as in situ transmission electron microscopy (TEM)<sup>1,2</sup> in the past few decades, researchers have gained enormous knowledge of the relationship between defect nucleation and the subsequent plastic deformation of nanosized materials.<sup>3–7</sup> Due to their small dimensions, nanosized crystalline structures are often synthesized to feature few to no preexisting dislocations,<sup>8,9</sup> rendering them dependent on the nucleation of fresh dislocations from their surfaces to relieve stress under plastic deformation. Molecular dynamics (MD) simulation studies have over the past two decades demonstrated that such surface nucleation events are possible only at ultrahigh stresses approaching the theoretical strength.<sup>10–13</sup> Concurrently, in situ nanomechanical experiments have been conducted to observe and measure the nucleation events in defect-scarce nanomaterials.<sup>8,14–24</sup> The role of different types of point defects, e.g., vacancies<sup>25</sup> and hydrogen interstitials,<sup>26</sup> in the activation energy of surface dislocation nucleation has been investigated. Other studies have investigated and found evidence of the interplay between diffusive and displacive plasticity.<sup>17–19</sup> These studies have collectively shown a strong temperature dependence and a weak strain-rate dependence of the dislocation nucleation strength at experimentally relevant strain rates ( $10^{-5}$  to  $10^{-1}$  s<sup>-1</sup>). While these behaviors have been established, the atomistic origins of these effects remain unresolved. An intriguing idea that has been proposed<sup>14</sup> but not validated is that the strong temperature dependence of the nucleation strength implies that preexisting defects other than dislocations, such as surface self-diffusion of point defects, could serve as a precursor to the surface dislocation nucleation

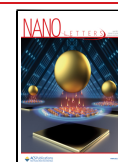
event itself.<sup>14,17,18,25,26</sup> Here, we conducted kinetic Monte Carlo (KMC) studies to investigate the central hypothesis that diffusion of point defects plays a fundamental role in surface dislocation nucleation in pristine crystalline nanomaterials. In doing so, we elucidate specific mechanisms by which the diffusion of a particular type of point defect, surface adatoms, directly impacts the incipient surface dislocation nucleation process.

We investigate Pd surface adatom diffusion-controlled incipient dislocation nucleation in truncated rhombic  $\langle 1\bar{1}0 \rangle$  Pd nanowires, with diameters ranging from 4 to 20 nm, and lengths of 16.5 nm, with tensile loading along the  $[1\bar{1}0]$  direction, as shown in Figure 1a. The nanowires have (100) and (111) transverse surfaces, the intersections of which as shown in the red lines in Figure 1a represent preferential dislocation nucleation sites, or “nucleation edges”, as previously shown in both MD simulations and experiments.<sup>14,16</sup> The overall KMC model comprises two separate but coupled KMC components. The first KMC component characterizes surface adatom diffusion, while the second KMC component characterizes surface dislocation nucleation. The two KMC components are coupled because the activation

Received: May 4, 2023

Revised: June 12, 2023

Published: June 14, 2023



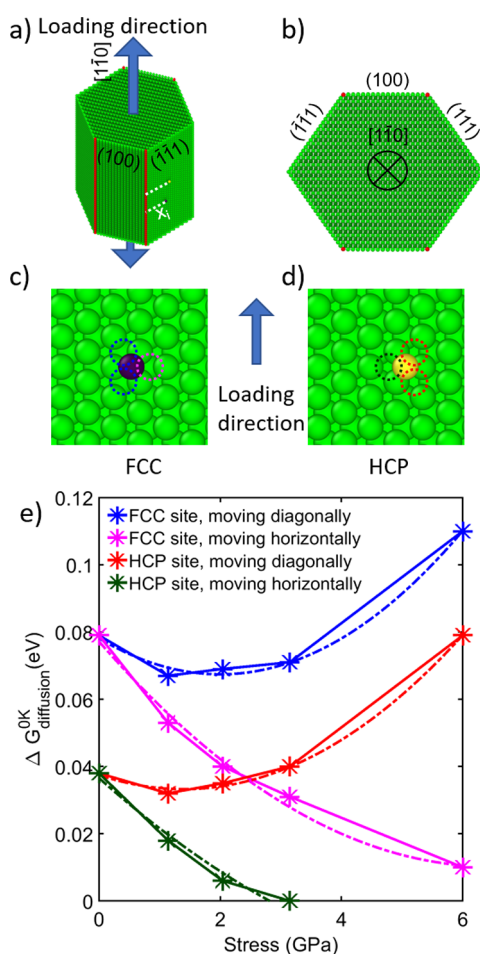


**Figure 1.** (a) Schematic representation of a  $\langle 1\bar{1}0 \rangle$ -oriented Pd nanowire used in the KMC simulation, featuring two adatoms situated near the center of the  $(\bar{1}\bar{1}1)$  surface. The white dotted lines indicate adatom locations  $x_i$ . The red lines on the front face and red dots on the back face denote potential dislocation nucleation sites under tensile stress when no adatoms are present. These sites are situated along intersecting edges between the  $\{100\}$  and  $\{111\}$  surfaces. (b) Cross-sectional view of the Pd nanowire (adatoms not shown). (c and d) Potential diffusion sites for adatoms when positioned at FCC and HCP sites, respectively. (e) Zero-temperature activation energy for diffusion, with the line color matching the site color in panels c and d. Dotted curves represent fitted curves of the respective CINEB simulation results.

energy for surface dislocation nucleation depends on the relative position of the surface adatom relative to the nucleation edges, which is determined by the KMC model of surface adatom diffusion. The KMC simulations do not account for structural relaxation after adatom diffusion, which could be accounted for by coupling MD and KMC. Each simulation maintains a constant system temperature ( $T$ ) and tensile loading strain rate ( $\dot{\epsilon}$ ). We maintain a constant areal surface adatom density of  $1.7 \times 10^{11} \text{ cm}^{-2}$ , ensuring the presence of at least one adatom in the smallest structures examined. For a 20 nm thick nanowire, this density corresponds to five adatoms per nanowire. The main text focuses on the results obtained from the 20 nm thick nanowire, while the Supporting Information provides a brief discussion and results on nanowires with varying thicknesses.

In experiments, adatom deposition is governed by a balance between kinetic and thermodynamic control.<sup>9</sup> At equilibrium

(thermodynamic dominant conditions), adatoms tend to remain away from edges due to their high-energy state. On the basis of this observation, we assume that at the start of each KMC run at zero applied external stress the adatom(s) are within 1 nm of the center of the  $(111)$  plane. We note that at experimentally relevant rates ( $10^{-5}$  to  $10^{-1} \text{ s}^{-1}$ ), the structure size, initial adatom distribution, and adatom density have minimal impact on the results, provided there is at least one adatom. However, for higher strain rates (i.e.,  $\dot{\epsilon} = 1 \text{ s}^{-1}$ ), these factors become increasingly important, particularly at lower temperatures. This will be discussed later in the context of strain-rate sensitivity.

The diffusion and nucleation KMC components consist of multiple attempts. In the diffusion KMC, an attempt involves an adatom diffusing to an adjacent site, as shown in panels c and d of Figure 1. If the attempt is successful, the new adatom position ( $x_i$  in Figure 1a) is updated. For the nucleation of KMC, an attempt corresponds to forming a Shockley partial dislocation loop. If successful, the KMC simulation is terminated, and the current stress,  $\sigma$ , is deemed to be the nucleation strength.

Each adatom diffusion attempt or surface dislocation nucleation attempt uses its respective activation free energy to evaluate the probability ( $p$ ) of an attempt's success:

$$p = \min \left[ 1, e^{-1/kT \times \Delta G_{\text{attempt}}^{0\text{K}}(\sigma) \left(1 - \frac{T}{T_m}\right)} \right] \quad (1)$$

where  $k$  is the Boltzmann constant and  $T$  and  $\sigma$  represent the current simulation temperature and stress, respectively.  $p$  is then compared to a random number from a uniform distribution in the  $(0, 1)$  interval. A successful attempt occurs when  $p$  is larger than the random number.  $T_m$  denotes the surface disordering temperature constant, for which we use a value of 914 K for Pd.<sup>14</sup> The zero-temperature activation energy,  $\Delta G_{\text{attempt}}^{0\text{K}}$  can be calculated using the Climbing Image Nudged Elastic Band (CINEB) method.<sup>10,27</sup> In this study, the Pd potential developed by Zhou et al.<sup>28</sup> has been utilized to perform the CINEB calculations. See the Supporting Information for further details on the CINEB and KMC setup.

As shown in Figure 1e,  $\Delta G_{\text{diffusion}}^{0\text{K}}(\sigma)$  is highly sensitive to the initial  $\{111\}$  site type (FCC site or HCP site) occupied by the adatom and the diffusion direction under applied tensile stress. In addition,  $\Delta G_{\text{nucleation}}^{0\text{K}}(\sigma)$ , illustrated in Figure 2a, is influenced by the adatom's location, which is determined by the diffusion component of the KMC and then used as input for the nucleation KMC.

The edges between intersecting  $\{001\}$  and  $\{111\}$  surfaces, termed "nucleation edges", are potential dislocation nucleation sites even in the absence of adatoms.<sup>14,16</sup> When an adatom is within 0.5 nm, i.e., in contact with a nucleation edge (see Figure 2b–d for an example), the activation free energy for dislocation nucleation is significantly reduced as shown in Figure 2a. This reduction can be attributed to the adatom's presence, which causes a substantial increase in local resolved shear stress from 0.11 GPa (Figure 2e) to 0.77 GPa (Figure 2b) even without external strain. This considerable increase in shear stress can be attributed to surface stress changes induced by the adatom. Consequently, the local stress increase facilitates incipient plastic deformation via Shockley partial nucleation near the adatom, as observed in Figure 2d. In contrast, without adatoms, incipient Shockley partial nucleation can occur at any location along the nucleation edge. Overall, as shown in Figure 2a, the  $\Delta G_{\text{nucleation}}^{0\text{K}}(\sigma)$  used to

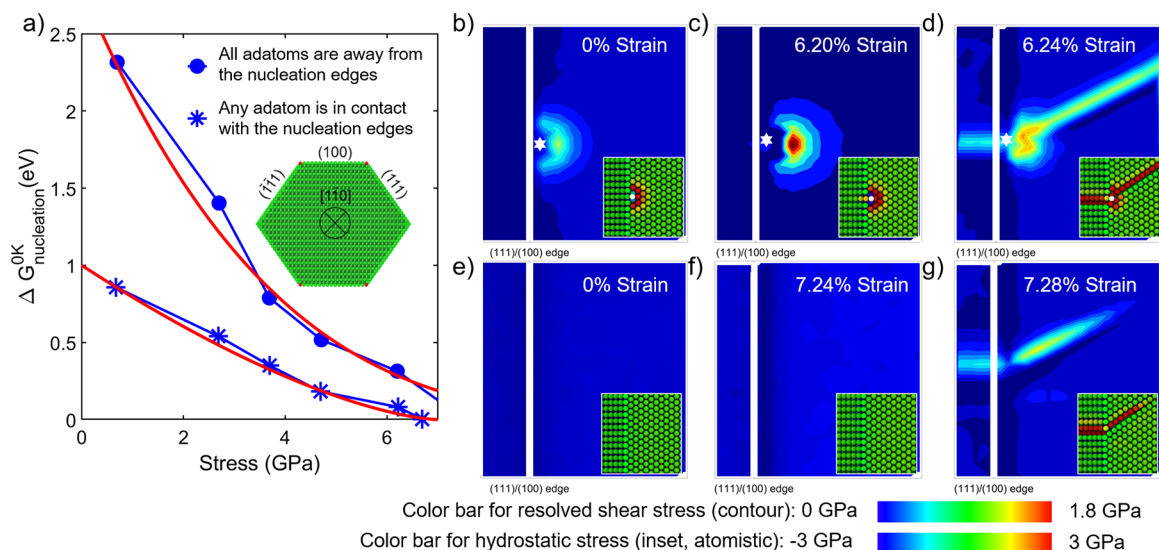


**Figure 2.** (a) Zero-temperature activation energy for surface dislocation nucleation based on the adatom location. The inset shows the nanowire cross section, with red dots indicating the (100)/(111) nucleation edges. The red curves are fitting curves based on CINEB simulation results. (b–d) Resolved shear stress contours near nucleation edges during MD tensile loading simulation with an adatom present (white hexagrams represent adatoms). (e–g) Resolved shear stress contours near nucleation edges during MD tensile loading simulation without an adatom. The insets in panels b–g display the corresponding atomic configurations color-coded by hydrostatic stress; the white atom in panels b–d marks the adatom location. White vertical lines in the figures highlight the (100)/(111) nucleation edges.

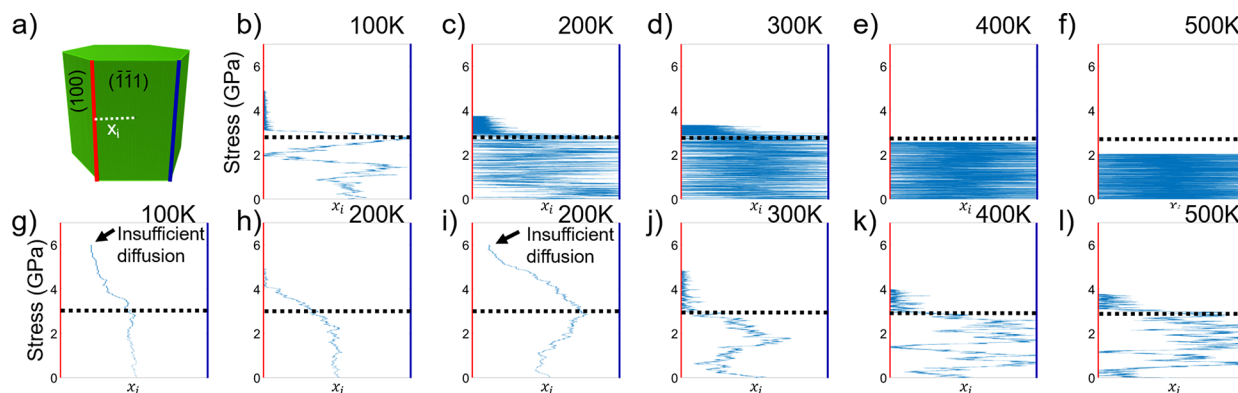


**Figure 3.** (a) Illustration of an adatom on a 20 nm diameter nanowire at the beginning of the KMC simulation. (b–f) Stress-dependent adatom diffusion trajectories leading to dislocation nucleation at various temperatures for strain rate  $\dot{\epsilon} = 10^{-4} \text{ s}^{-1}$ . (g–l) Similar stress-dependent trajectories for strain rate  $\dot{\epsilon} = 1 \text{ s}^{-1}$ . (h) Case in which an adatom reaches the nucleation edge, facilitating nucleation. (i) Case in which the adatom does not reach the nucleation edge to facilitate nucleation. Cases h and i occur under the same strain rate and temperature. Although multiple adatoms diffuse on each nanowire due to the constant adatom density and larger nanowire diameter, only one trajectory is plotted for the sake of clarity. Black dashed lines denote the critical adatom trapping stress from Figure 1e. Vertical red lines denote the (100)/(111) edges, and vertical blue lines denote the (111)/(111) edges.

evaluate nucleation attempts depends on the adatom's proximity to the nucleation edge; if the adatom is in contact (i.e., within 0.5 nm) with the nucleation edge, the higher stress-dependent activation energy in Figure 2a is used, while if not in contact, the lower activation energy is employed. We note that in our KMC simulations, adatoms are assumed to diffuse independently of each other during the diffusion phase. Furthermore, defect nucleation during the nucleation stage is assumed to occur in the presence of a single adatom.

We note that the activation energies for nucleation, both with and without adatoms, exhibit differences not only in magnitude but also in their stress dependencies, as illustrated in Figure 2a. For a direct comparison of the stress dependence, we introduce the common exponential dependence as<sup>10,14</sup>

$$\Delta G_{\text{nucleation}}^{0K}(\sigma) = \Delta U_{\text{act}} \left( 1 - \frac{\sigma}{\sigma_{\text{athermal}}} \right)^{\alpha} \quad (2)$$

where  $\sigma_{\text{athermal}}$  represents the athermal strength limit. In our KMC model, we obtained the value of  $\alpha$  directly from the fitting curves in Figure 2a. In the absence of adatoms,  $\alpha$  has a value of 3.92, consistent with CINEB calculations on edge dislocation nucleation in a  $\langle 110 \rangle$ -oriented Cu nanowire under tension<sup>10</sup> without adatoms. Including adatoms, however, reduces  $\alpha$  to 1.56, signifying a weakened stress dependence.

This reduction in  $\alpha$  stems from adatoms assisting in Shockley partial nucleation, creating locally concentrated stress fields that are less sensitive to applied stress. As depicted in panels b and c of Figure 2, the local resolved shear stress around the adatom only increases from 0.77 to 1.74 GPa

before yielding, while the applied tensile stress increases from 0 to 4.56 GPa. In contrast, when adatoms are absent, the applied tensile stress acts as the sole driving force for dislocation nucleation, leading to a stronger stress dependence.

Having established the KMC diffusion and nucleation models, we can now discuss the new mechanistic insights they offer into the role of surface diffusion in surface dislocation nucleation. Specifically, Figure 1e demonstrates that for tensile stresses exceeding  $\sim 3.1$  GPa,  $\Delta G_{\text{diffusion}}^0(\sigma)$  for an HCP site adatom moving horizontally becomes zero and remains so, indicating that adatoms will prefer to diffuse in a specific direction (e.g., to the left, following the site/direction schematic notations in panels c and d of Figure 1 and in Figure 3). This preferential movement ultimately leads to adatoms being “trapped” near nucleation edges when the applied stress exceeds the critical stress.

The critical stress for adatom trapping depends on the nanowire size and temperature and is typically  $\sim 3$  GPa for the considered nanowire diameters (5–20 nm). For the experimentally relevant strain rates of  $10^{-5}$  to  $10^{-1}$  s $^{-1}$ , panels b–f of Figure 3 illustrate how, for a given temperature, an individual adatom diffuses along the surface as a function of the applied tensile stress. Specifically, the adatoms tend to diffuse across the entire {111} surface numerous times before reaching the critical stress. However, when approaching or exceeding the critical stress, adatoms become trapped near nucleation edges due to the emergence of preferential diffusion directions. This trapping process significantly reduces the activation energy for surface dislocation nucleation, as shown in Figure 2a. Interestingly, we also found that the decrease in activation energy facilitated by surface adatoms is dependent on nanowire diameter and surface morphology and further that this effect becomes weaker as the nanowire edges become more rounded. However, it is important to note that this effect does not entirely vanish, even in the extreme case of nanowires with round cross sections.

At strain rates of  $10^{-5}$  to  $10^{-1}$  s $^{-1}$  in Figure 3b–f, the trapping mechanism exhibits temperature sensitivity, as the likelihood of thermally induced events enabling adatoms to diffuse away from nucleation edges decreases at lower temperatures. As a result, panels b–d of Figure 3 demonstrate a closer trapping of adatoms near nucleation edges at lower temperatures, which promotes yielding through adatom-facilitated nucleation events. Conversely, the trapping mechanism becomes less prominent at higher temperatures (400 and 500 K in panels e and f, respectively, of Figure 3) due to a combination of lower yielding stress and a higher probability of diffusive events in all directions.

While the trapping mechanism becomes less dominant at higher temperatures, the high diffusion attempt frequency ( $\sim 10^{12}$  attempts per second, calculation details in the Supporting Information) and a higher likelihood of diffusion events being accepted at higher temperatures enable adatoms to frequently reach the nucleation edges at higher temperatures. In conjunction with the high dislocation nucleation attempt frequency and the significant reduction in nucleation activation energy due to the presence of adatoms, this implies that adatom-facilitated nucleation events still dominate the yielding of nanowires at higher temperatures. In fact, all successful nucleation events at low strain rates ( $10^{-5}$  to  $10^{-1}$  s $^{-1}$ ) in our KMC simulations involve adatoms in contact with the nucleation edges (i.e., adatom-facilitated nucleation events).

We now discuss the impact of strain rate on the stress-regulated diffusion mechanism; panels g–l of Figure 3 illustrate the distinct behavior that occurs starting at a strain rate of  $\sim 1$  s $^{-1}$ . Higher-temperature results (300, 400, and 500 K) show only adatom-facilitated nucleation events resulting from the occurrence of the adatom trapping mechanism, mirroring the low-strain-rate outcomes in Figure 3b–f. However, at 200 K, no-adatom-facilitated events begin to emerge, becoming as favorable as adatom-facilitated events. This is because with an increase in strain rate, fewer diffusion attempts can occur before the applied stress reaches a level at which the activation energy for nucleation without adatoms becomes sufficiently low, making it challenging for adatoms to reach the nucleation edge before stress-induced yielding occurs. This transition arises as a consequence of the increasing strain rate, which reduces the time for diffusion before the applied stress attains a level at which the activation energy for nucleation without adatoms becomes sufficiently low. In other words, it becomes harder for adatoms to reach the nucleation edge prior to stress-induced yielding as the strain rate increases. This contrasts starkly with a strain rate of  $10^{-4}$  s $^{-1}$ , where the nanowire takes 10 000 times longer to achieve the same strain as at a strain rate of 1 s $^{-1}$ . This elongated period allows surface adatoms ample time to diffuse, enabling an extended back-and-forth movement along the surface. Consequently, the wider diffusion range observed at a strain rate of  $10^{-4}$  s $^{-1}$ , compared to 1 s $^{-1}$ , is a direct result of this prolonged diffusion opportunity. We thus predict that an increase in strain rates above 1 s $^{-1}$  would further increase the temperature threshold for the dominance of stress-induced nucleation events compared to adatom-facilitated nucleation events.

We note that the nucleation strength prediction of the KMC diffusion–nucleation model, as illustrated in Figure 4, demonstrates reasonable agreement with both the experimental data and the analytical model from Chen et al.<sup>14</sup> for

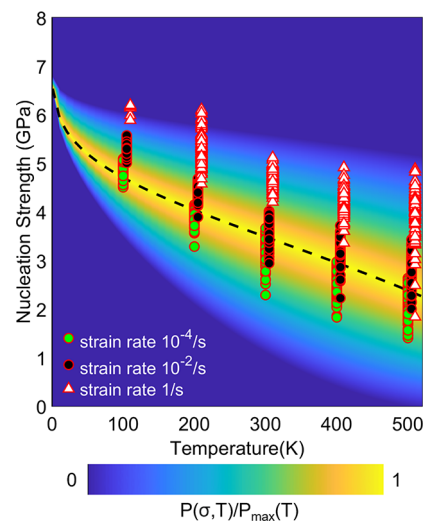


**Figure 4.** Predicted nucleation strength under varying temperatures and strain rates from the KMC model. The background color map illustrates the temperature-dependent normalized probability distribution function, while the dashed black line indicates the most probable nucleation strength, both based on the analytical model proposed by Chen et al.<sup>14</sup> for a strain rate of  $10^{-4}$  s $^{-1}$  and an  $\alpha$  of 4. Probability values  $P(\sigma, T)$  are normalized in relation to the highest probability at each specific temperature [ $P_{\text{max}}(T)$ ].

truncated-rhombic Pd nanowires at a similar strain rate ( $\sim 10^{-4}$  s $^{-1}$ ). Furthermore, the KMC model captures key features previously observed experimentally,<sup>14</sup> such as the high nucleation strength approaching the theoretical limit at low temperatures, the weak strain-rate dependence from  $10^{-4}$  to  $10^{-3}$  s $^{-1}$ , and the significant scattering of nucleation strength due to the temperature-driven stochastic nature of the adatom-controlled surface dislocation nucleation process. As the strain rate increases to the transitional strain rate (1 s $^{-1}$ ), a shift in nucleation strength occurs due to the relative lack of adatom diffusion discussed above. This effect is particularly evident at 200 K, where both adatom-facilitated and no-adatom-facilitated nucleation events occur with similar ratios, resulting in further scattering in nucleation strength, as seen in Figure 4. Furthermore, by taking the derivative of  $\Delta G_{\text{nucleation}}$  with respect to stress  $\sigma$ , we are able to determine the changes in activation volumes<sup>10,29</sup> for the two distinct nucleation energy curves displayed in Figure 2a. We find that the activation volume for adatom-facilitated nucleation falls in the range of 1–5  $b^3$ . Similarly, for nucleation that occurs without adatom facilitation, the activation volume ranges from 1 to 10  $b^3$ . This indicates that in both cases, nucleation originates from a surface source as opposed to a bulk source such as the Frank–Read source, which typically involves activation volumes between 100 and 1000  $b^3$ .

Finally, we note that this study primarily examines truncated rhombic Pd nanowires. However, the generality of our findings for other FCC metals depends on the condition that the energy barrier for diffusion, as shown in Figure 1e, decreases to zero as the applied stress increases, thereby facilitating the adatom trapping mechanism discussed herein. Preliminary results indicate that the energy barrier for diffusion decreasing to zero with increasing stress is found for a wide range of stacking fault energies. Thus, we anticipate that the exact nature of the initial nucleation event should not significantly affect the relevance of our conclusions to other FCC metals.

In summary, we have developed a KMC model to investigate the previously proposed hypothesis of temperature- or diffusion-assisted defect nucleation in truncated rhombic Pd nanowires. By capturing the fact that the diffusion of adatoms becomes directionally biased at a critical applied stress level, we provide a mechanistic understanding of experimental observations of strong temperature dependence and low strain-rate dependence at experimentally relevant strain rates ( $10^{-5}$  to  $10^{-1}$  s $^{-1}$ ), as well as the temperature-dependent scatter in the surface dislocation nucleation strength. Furthermore, the model demonstrates that a decreasing rate of adatom diffusion with an increasing strain rate will lead to stress-controlled nucleation being the dominant nucleation mechanism at higher strain rates. Overall, we demonstrate the significant influence that adatom diffusion can have on the incipient defect nucleation processes in metal nanowires.

## ■ ASSOCIATED CONTENT

### SI Supporting Information

The Supporting Information is available free of charge at <https://pubs.acs.org/doi/10.1021/acs.nanolett.3c01660>.

Detailed descriptions of the CINEB and KMC setups used in our study and a brief discussion of the size effect (PDF)

## ■ AUTHOR INFORMATION

### Corresponding Author

Harold S. Park – Department of Mechanical Engineering, Boston University, Boston, Massachusetts 02215, United States; [orcid.org/0000-0001-5365-7776](https://orcid.org/0000-0001-5365-7776); Email: [parkhs@bu.edu](mailto:parkhs@bu.edu)

### Authors

Lijie He – Department of Mechanical Engineering, Boston University, Boston, Massachusetts 02215, United States; [orcid.org/0000-0002-6275-7995](https://orcid.org/0000-0002-6275-7995)

Guangming Cheng – Department of Mechanical and Aerospace Engineering, North Carolina State University, Raleigh, North Carolina 27695, United States; [orcid.org/0000-0001-5852-1341](https://orcid.org/0000-0001-5852-1341)

Yong Zhu – Department of Mechanical and Aerospace Engineering, North Carolina State University, Raleigh, North Carolina 27695, United States

Complete contact information is available at:

<https://pubs.acs.org/doi/10.1021/acs.nanolett.3c01660>

### Notes

The authors declare no competing financial interest.

## ■ ACKNOWLEDGMENTS

All authors acknowledge the support of the National Science Foundation via Grants CMMI-1929651 and CMMI-1929646.

## ■ REFERENCES

- (1) Hirsch, P. B.; Horne, R. W.; Whelan, M. J. LXVIII. Direct observations of the arrangement and motion of dislocations in aluminium. *Philos. Mag.* **1956**, *1*, 677–684.
- (2) Minor, A. M.; Dehm, G. Advances in in situ nanomechanical testing. *MRS Bull.* **2019**, *44*, 438–442.
- (3) Lu, Y.; Song, J.; Huang, J. Y.; Lou, J. Surface dislocation nucleation mediated deformation and ultrahigh strength in sub-10-nm gold nanowires. *Nano Research* **2011**, *4*, 1261–1267.
- (4) Jennings, A. T.; Li, J.; Greer, J. R. Emergence of strain-rate sensitivity in Cu nanopillars: Transition from dislocation multiplication to dislocation nucleation. *Acta Mater.* **2011**, *59*, S627–S637.
- (5) Zheng, H.; Cao, A.; Weinberger, C. R.; Huang, J. Y.; Du, K.; Wang, J.; Ma, Y.; Xia, Y.; Mao, S. X. Discrete plasticity in sub-10-nm-sized gold crystals. *Nat. Commun.* **2010**, *1*, 144.
- (6) Schuh, C. A.; Mason, J. K.; Lund, A. C. Quantitative insight into dislocation nucleation from high-temperature nanoindentation experiments. *Nat. Mater.* **2005**, *4*, 617–621.
- (7) Oh, S. H.; Legros, M.; Kiener, D.; Dehm, G. In situ observation of dislocation nucleation and escape in a submicrometre aluminium single crystal. *Nat. Mater.* **2009**, *8*, 95–100.
- (8) Richter, G.; Hillerich, K.; Gianola, D. S.; Mönig, R.; Kraft, O.; Volkert, C. A. Ultrahigh strength single crystalline nanowhiskers grown by physical vapor deposition. *Nano Lett.* **2009**, *9*, 3048–3052.
- (9) Xia, Y.; Xia, X.; Peng, H. C. Shape-Controlled Synthesis of Colloidal Metal Nanocrystals: Thermodynamic versus Kinetic Products. *J. Am. Chem. Soc.* **2015**, *137*, 7947–7966.
- (10) Zhu, T.; Li, J.; Samanta, A.; Leach, A.; Gall, K. Temperature and strain-rate dependence of surface dislocation nucleation. *Phys. Rev. Lett.* **2008**, *100*, 025502.
- (11) Li, J.; Van Vliet, K. J.; Zhu, T.; Yip, S.; Suresh, S. Atomistic mechanisms governing elastic limit and incipient plasticity in crystals. *Nature* **2002**, *418*, 307–310.
- (12) Warner, D. H.; Curtin, W. A. Origins and implications of temperature-dependent activation energy barriers for dislocation nucleation in face-centered cubic metals. *Acta Mater.* **2009**, *57*, 4267–4277.

- (13) Park, H. S.; Gall, K.; Zimmerman, J. A. Deformation of FCC nanowires by twinning and slip. *Journal of the Mechanics and Physics of Solids* **2006**, *54*, 1862–1881.
- (14) Chen, L. Y.; He, M. R.; Shin, J.; Richter, G.; Gianola, D. S. Measuring surface dislocation nucleation in defect-scarce nanostructures. *Nat. Mater.* **2015**, *14*, 707–713.
- (15) Chang, T. H.; Cheng, G.; Li, C.; Zhu, Y. On the size-dependent elasticity of penta-twinned silver nanowires. *Extreme Mechanics Letters* **2016**, *8*, 177–183.
- (16) Yin, S.; Cheng, G.; Richter, G.; Gao, H.; Zhu, Y. Transition of Deformation Mechanisms in Single-Crystalline Metallic Nanowires. *ACS Nano* **2019**, *13*, 9082–9090.
- (17) Zhong, L.; Sansoz, F.; He, Y.; Wang, C.; Zhang, Z.; Mao, S. X. Slip-activated surface creep with room-temperature super-elongation in metallic nanocrystals. *Nat. Mater.* **2017**, *16*, 439–445.
- (18) Ramachandramoorthy, R.; Wang, Y.; Aghaei, A.; Richter, G.; Cai, W.; Espinosa, H. D. Reliability of Single Crystal Silver Nanowire-Based Systems: Stress Assisted Instabilities. *ACS Nano* **2017**, *11*, 4768–4776.
- (19) Sun, S.; Kong, D.; Li, D.; Liao, X.; Liu, D.; Mao, S.; Zhang, Z.; Wang, L.; Han, X. Atomistic Mechanism of Stress-Induced Combined Slip and Diffusion in Sub-5 Nanometer-Sized Ag Nanowires. *ACS Nano* **2019**, *13*, 8708–8716.
- (20) Seo, J. H.; Yoo, Y.; Park, N. Y.; Yoon, S. W.; Lee, H.; Han, S.; Lee, S. W.; Seong, T. Y.; Lee, S. C.; Lee, K. B.; Cha, P. R.; Park, H. S.; Kim, B.; Ahn, J. P. Superplastic deformation of defect-free Au nanowires via coherent twin propagation. *Nano Lett.* **2011**, *11*, 3499–3502.
- (21) Seo, J. H.; Park, H. S.; Yoo, Y.; Seong, T. Y.; Li, J.; Ahn, J. P.; Kim, B.; Choi, I. S. Origin of size dependency in coherent-twin-propagation-mediated tensile deformation of noble metal nanowires. *Nano Lett.* **2013**, *13*, 5112–5116.
- (22) Lee, S.; Im, J.; Yoo, Y.; Bitzek, E.; Kiener, D.; Richter, G.; Kim, B.; Oh, S. H. Reversible cyclic deformation mechanism of gold nanowires by twinning-detwinning transition evidenced from in situ TEM. *Nat. Commun.* **2014**, *5*, 3033.
- (23) Cheng, G.; Yin, S.; Li, C.; Chang, T. H.; Richter, G.; Gao, H.; Zhu, Y. In-situ TEM study of dislocation interaction with twin boundary and retraction in twinned metallic nanowires. *Acta Mater.* **2020**, *196*, 304–312.
- (24) Cheng, G.; Yin, S.; Chang, T. H.; Richter, G.; Gao, H.; Zhu, Y. Anomalous Tensile Detwinning in Twinned Nanowires. *Phys. Rev. Lett.* **2017**, *119*, 256101.
- (25) Qin, Q.; Yin, S.; Cheng, G.; Li, X.; Chang, T. H.; Richter, G.; Zhu, Y.; Gao, H. Recoverable plasticity in penta-twinned metallic nanowires governed by dislocation nucleation and retraction. *Nat. Commun.* **2015**, *6*, 5983.
- (26) Yin, S.; Cheng, G.; Chang, T. H.; Richter, G.; Zhu, Y.; Gao, H. Hydrogen embrittlement in metallic nanowires. *Nat. Commun.* **2019**, *10*, 2004.
- (27) Henkelman, G.; Uberuaga, B. P.; Jónsson, H. Climbing image nudged elastic band method for finding saddle points and minimum energy paths. *J. Chem. Phys.* **2000**, *113*, 9901–9904.
- (28) Zhou, X. W.; Johnson, R. A.; Wadley, H. N. G. Misfit-energy-increasing dislocations in vapor-deposited CoFe/NiFe multilayers. *Phys. Rev. B* **2004**, *69*, 144113.
- (29) Zhang, X.; Li, X.; Gao, H. Size and strain rate effects in tensile strength of penta-twinned Ag nanowires. *Acta Mechanica Sinica* **2017**, *33*, 792–800.

## Recommended by ACS

### Nucleation of Threading Dislocations in 4H-SiC at Early Physical-Vapor-Transport Growth Stage

Qinqin Shao, Rong Wang, *et al.*

JUNE 05, 2023  
CRYSTAL GROWTH & DESIGN

READ 

### In Situ Atomic-Scale Observation of 5-Fold Twin Formation in Nanoscale Crystal under Mechanical Loading

Xiang Wang, Scott X. Mao, *et al.*

JANUARY 12, 2023  
NANO LETTERS

READ 

### Dislocation Climb in AlN Crystals Grown at Low-Temperature Gradients Revealed by 3D X-ray Diffraction Imaging

Thomas Straubinger, Carsten Richter, *et al.*

JANUARY 26, 2023  
CRYSTAL GROWTH & DESIGN

READ 

### Discovery of Double Helix and Impact on Nanoscale to Mesoscale Crystalline Structures

Jagdish Narayan and Roger Narayan

JULY 18, 2022  
ACS OMEGA

READ 

Get More Suggestions >